High-dimensional characterization of IL-10 production and IL-10 dependent regulation during primary gammaherpesvirus infection

Abigail K. Kimball[1], Lauren M. Oko[2], Rachael E. Kaspar[1], Linda F. van Dyk[2], and Eric T. Clambey[1]*

[1] Department of Anesthesiology and [2]Department of Immunology and Microbiology, University of Colorado Denver, Anschutz Medical Campus, Aurora, CO 80045

* Address correspondence and reprint requests to Dr. Eric T. Clambey, Department of Anesthesiology, School of Medicine, University of Colorado Anschutz Medical Campus, 12700 E. 19th Ave., Box 112, Aurora, CO, 80045. E-mail address: Eric.Clambey@ucdenver.edu

ORCIDs: 0000-0002-9831-386X (A.K.K.); 0000-0002-7125-7036 (L.M.O.); 0000-0002-1181-7919 (R.E.K.); 0000-0003-2662-5554 (L.F.v.D.); 0000-0002-7972-9544 (E.T.C.).

This work was funded by National Institutes of Health Grants R01 AI121300 and R01 CA168558 (to L.F.v.D.), an American Heart Association National Scientist Development grant (#13SDG14510023), the Crohn's and Colitis Foundation of America (#311295), a pilot grant from the Lung, Head and Neck Cancer program within the University of Colorado Cancer Center, and a Career Enhancement Award from the University of

Colorado Lung Cancer Specialized Program of Research Excellence (P50CA58187) (all to E.T.C.).

The Lung, Head and Neck program within the University of Colorado Cancer Center, and the Flow Cytometry Shared Resource, are directly funded through support from the National Cancer Institute Cancer Center Support Grant P30CA046934.

Abbreviations used in this article: B6, C57BL/6; CyTOF, cytometry by time-of-flight; γHV68, murine gammaherpesvirus 68; IFNγ, Interferon-gamma, IL-10, Interleukin-10; ICCS, Intracellular cytokine stain; KO, knockout; TNFα, tumor necrosis factor-alpha, tSNE, t-distributed stochastic neighbor embedding.

ABSTRACT

Interleukin (IL)-10 is a potent immunomodulatory cytokine produced by multiple cell types to restrain immune activation. Many herpesviruses have utilized the IL-10 pathway to facilitate infection, but how endogenous IL-10 is regulated during primary infection in vivo remains poorly characterized. Here, we infected mice with murine gammaherpesvirus 68 (γHV68) and analyzed the production, and genetic contribution, of IL-10 using mass cytometry, or cytometry by time-of-flight (CyTOF), analysis. γHV68 infection elicited a breadth of effector CD4 T cells in the lungs of acutely infected mice, including a highly activated effector subset that co-expressed IFNγ, TNFα, and IL-10. By using IL-10 green fluorescent protein (gfp) transcriptional reporter mice, we identified that IL-10 was primarily expressed within CD4 T cells during acute infection in the lungs. IL10gfp expressing CD4 T cells were highly proliferative and characterized by the expression of multiple co-inhibitory receptors including PD-1 and LAG-3. When we analyzed acute γHV68 infection of IL-10 deficient mice, we found that IL-10 limits the frequency of both myeloid and effector CD4 T cell subsets in the infected lung, with minimal changes at a distant mucosal site. These data emphasize the unique insights that high-dimensional analysis can afford in investigating antiviral immunity, and provide new insights into the breadth, phenotype and function of IL-10 expressing effector CD4 T cells during acute virus infection.

INTRODUCTION

The gammaherpesviruses (γHVs) are a group of large dsDNA lymphotropic viruses which include the human pathogens Epstein-Barr virus (EBV) and Kaposi's sarcoma associated herpesvirus (KSHV), and the small animal model murine gammaherpesvirus 68 (γHV68) (1-3). The γHVs establish a lifelong infection in their host, with most infections in immunocompetent hosts asymptomatic. In contrast, immunosuppressed individuals are at a significantly increased risk for the development of a variety of chronic pathologies, including γHV-associated malignancies (4).

γHV infection is critically regulated by the immune system, and γHVs have evolved numerous strategies to either subvert or avoid immune destruction, thereby facilitating lifelong infection (5-7). Among these, IL-10 is a multifunctional cytokine that downregulates the expression of multiple pro-inflammatory cytokines and cell surface molecules, and can influence a wide array of immune cell types (8-10). IL-10 is a frequent target of manipulation by the herpesviruses, with some γHVs, like Epstein-Barr virus (EBV), encoding their own IL-10 homolog (11, 12), whereas other viruses, including murine gammaherpesvirus 68 (γHV68), inducing cellular IL-10 (13). IL-10 has been reported to regulate multiple aspects of γHV68 infection. For instance, γHV68-infected IL-10 deficient mice fail to control leukocytosis, have greater splenomegaly and a reduced latent load (14), with these mice susceptible to an exacerbated inflammatory bowel disease (15). IL-10 has been reported to be induced in B cells by the γHV68 M2 gene product (13). IL-10 expressing CD8 T cells have also been observed during chronic γHV68 infection in mice depleted for CD4 T cells, an immunosuppressive phenotype associated with chronic viral pathogenesis (16).

77 The above reports identified a clear role for IL-10 in shaping the outcome of
78 γHV68 infection. Here we applied high-dimensional, single-cell analysis using mass
79 cytometry (cytometry by time-of-flight, CyTOF) (17) to define the breadth and cellular
80 phenotype of IL-10 expressing cells elicited during acute γHV68 infection. We further
81 analyzed the genetic impact of IL-10 in limiting γHV68 induced inflammation. These
82 studies demonstrate the acute impact of IL-10 on primary γHV infection in vivo and
83 define effector CD4 T cells as a major cell source of IL-10 during acute pulmonary
84 infection.

MATERIALS AND METHODS

Experimental samples. Mice were obtained from the Jackson Laboratory and bred in-house at the University of Colorado, including the C57BL/6J (B6, Jax stock #000664), IL10-deficient (IL10KO, B6.129P2-*Il10*^{tm1Cgn}/J, Jax stock #002251), or IL10gfp (B6.129S6-*Il10*^{tm1Flv}/J, Jax stock #008379) genotypes. Mice were intranasally infected with $4x10^5$ plaque forming units (PFU) of wild-type (WT) murine gammaherpesvirus 68 (γHV68) in mice subjected to isoflurane induced anesthesia. Mice were used between 8-15 weeks of age, with experimental cohorts age- and sex-matched. Mice were infected with WT γHV68 (strain WUMS, ATCC VR-1465) (18), using either bacterial artificial chromosome (BAC)-derived WT γHV68 (19) or WT γHV68.ORF73βla, which encodes a fusion between ORF73 and the beta-lactamase gene (20). γHV68 was grown and titered by plaque assay on NIH 3T12 fibroblasts as previously published (21). Mice subjected to anti-CD3 antibody injection were injected intraperitoneally with 15 μg of anti-CD3ε antibody (clone 145-2C11, BioXcell, Cat# BP0001-1) at 0 and 46 hours, with spleens harvested at 50 hours post primary injection (22). Lung data in Figure 4 are from a previously published dataset (23). All procedures were performed under protocols approved by the Institutional Animal Care and Use Committee at the University of Colorado Anschutz Medical Campus.

Cell processing & antibody staining. In-depth processing and staining protocol can be found in (23). Briefly, lungs were perfused using 10-12 mL of phosphate buffered saline (PBS), harvested, minced and enzymatically digested with collagenase D for 1 h at

37°C. Lungs, and spleens, were further subjected to mechanical disruption to generate single-cell suspensions that were subjected to red blood cell lysis, and resuspended for staining. Colons were surgically dissected, rinsed then vortexed in PBS to remove fecal material, and incubated with PBS containing 15 mM HEPES, 1 mM EDTA at room temperature for 15 minutes while samples were vigorously vortexed, to remove intraepithelial lymphocytes. Colonic tissue was then rinsed over a sieve, washed with ice cold PBS, minced and subjected to enzymatic digestion using Collagenase VIII (100-200 units/mL final concentration, Sigma Aldrich) diluted in RPMI 1640 (Gibco) supplemented with 5% fetal bovine serum, 15 mM HEPES, and 1% penicillin/streptomycin. Enzymatic digestion was quenched using ice cold RPMI 1640 with 5% fetal bovine serum. Colonic samples were washed with a 1:10,000 dilution of Benzonase® Nuclease (≥250 units/µL, Sigma Aldrich) in RPMI 1640 to minimize cell aggregation, prior to staining with cisplatin as a live/dead discriminator. For samples analyzed for intracellular cytokine staining, cells were pharmacologicaly stimulated with PMA and ionomycin in the presence of the Golgi apparatus inhibitors brefeldin A and monensin for 5 hours. Cells were stained with cisplatin according to manufacturer's recommendations (Cell-ID^{TM} Cisplatin, Fluidigm), incubated with Fc receptor blocking Ab (clone 2.4G2, Tonbo Biosciences) for 10-20 min, stained with primary surface Abs for 30 min at 22°C or 15 min at 37°C and 15 min at 22°C. Secondary surface stains, to detect fluorophore conjugated antibodies, were incubated for 20-30 min, and washed, with intracellular staining done using the FoxP3 Fix/Perm Buffer kit (Thermo Fisher) for 2 hours or overnight at 4°C. Following cell staining, cells were washed and resuspended in Intercalator (Cell-ID™ Intercalator-Ir). A subset of experiments (Figures 1, 3, 4B, 4D,

4F, and 5) were subjected to isotopic barcoding using the Fluidigm barcoding kit (Cell-ID™ 20-Plex Pd Barcoding Kit, Fluidigm) prior to staining with the primary surface stains. Antibodies used for these studies are listed in Tables 1-4B. All antibodies that were directly conjugated to isotopically purified elements were obtained from Fluidigm. In each of the CyTOF panels, a subset of antibodies were detected using a secondary detection approach, with FITC, PE, APC or Biotin-conjugated antibodies (clone and source identified in Tables 1-4B), detected using metal conjugated secondary antibodies against FITC, PE, APC or Biotin (Fluidigm).

CyTOF run and sample normalization/debarcoding. Samples were collected on a Helios mass cytometer (Fluidigm), with samples resuspended with equilibration beads to allow for signal normalization, with the normalization software downloaded from the Nolan laboratory GitHub page (https://github.com/nolanlab) (as in (23)). For experiments where the samples were subjected to isotopic barcoding (Figures 1, 3, 4B, 4D, 4F, and 5) the debarcoding software was used following normalization (https://github.com/nolanlab/single-cell-debarcoder). Normalized, debarcoded data were subjected to traditional Boolean gating in FlowJo, identifying singlets (^{191}Iridium (Ir)+ ^{193}Ir+) that were viable (^{195}Platinum(Pt)−). These events were then gated and exported for downstream analysis. Additional Boolean gating was later performed for either CD45+ events or CD4+ T cell events, with gating criteria identified within each figure.

PhenoGraph-based data analysis. Manually gated singlet (^{191}Ir+ ^{193}Ir+) viable (^{195}Pt−) events, or further gated populations, were imported into PhenoGraph, with relevant

clustering markers selected (28-35 cellular markers depending on the experiment; note that markers used for gating imported populations were not used for clustering). All parameters used for clustering are indicated in the associated Tables. PhenoGraph was run with the following settings: 1) files were merged using either the merge method "min" (Figure 1, Figure 2A, and Figure 3), all (Figure 2B), or "ceiling" (Figure 3-5), 2) files were transformed using the transformation method "cytofAsinh", 3) the "Rphenograph" clustering method was chosen, coupled with the "tSNE" visualization method. All other settings were automatically chosen, using default PhenoGraph settings.

PhenoGraph-based visualization. PhenoGraph-defined clusters were displayed on tSNE plots within the R package "Shiny" (23). Within the "Shiny" application, cluster color was altered or colored according protein expression. Multiple .csv files were produced by PhenoGraph, including "cluster median data" and "cluster cell percentage," which were used to determine cluster phenotype, distribution between conditions, and statistical significance between groups.

Software used and statistical analysis. Software for data analysis included: R studio (Version 1.1.453), downloaded from the official R website (http://www.r-project.org/); the Cytofkit package (Version 3.7), downloaded from Bioconductor (https://Bioconductor.org/packages/release/bioc/html/cytofkit.html), Excel 16.15, FlowJo 10.4.2, GraphPad Prism 7.0c, and Adobe Illustrator CC 22.1. Cytofkit was opened using R studio and XQuartz. Statistical significance was tested in GraphPad Prism using an

177 unpaired t test, with statistical significance as identified. For contexts in which we tested
178 statistical significance across all of the identified nodes/clusters (Fig. 4, 5), statistical
179 analysis was subjected to multiple comparison correction in GraphPad Prism.

RESULTS

High-dimensional analysis of effector CD4 T cells during primary γHV68 infection.

γHV68 infection induces diverse effector CD4 T cell subsets throughout the course of infection (24). To provide a high-dimensional analysis of effector CD4 T cell function during primary infection, the lungs from γHV68 infected mice were harvested at 9 days post-infection (dpi), subjected to pharmacological stimulation with PMA and ionomycin, and analyzed by mass cytometry using a panel of 35 isotopically purified, metal conjugated antibodies (Table 1). CD4 T cells were initially analyzed for expression of IFNγ and TNFα expression, two hallmark effector cytokines elicited in antiviral CD4 T cells. Between 40-60% of CD4 T cells harvested from infected lungs expressed either IFNγ, TNFα, or co-expressed IFNγ and TNFα (Fig. 1A). IFNγ+TNFα+ effector CD4 T cells were more frequent than either IFNγ+ or TNFα+ single positive cells (Fig. 1A). To gain an unbiased perspective on the phenotypic diversity within these cytokine-defined effector CD4 T cells, we next subjected these cell populations to the PhenoGraph algorithm, to define cell clusters present in each cytokine-defined subset (25). By clustering cells based on the expression of 30 proteins (including CD44, Tbet, IRF4 and multiple co-inhibitory receptors, but not on CD3, CD4, MHCII, IFNγ or TNFα) (Table 1), PhenoGraph defined 16 CD4 T cell clusters present in the virally infected lung (Fig. 1A-B). The relative frequency of these cell clusters was notably affected by whether cells expressed cytokines, and if so, which cytokines. Some clusters, depicted by shades of gray in Fig. 1B, were present in relatively comparable frequencies across all subsets of CD4 T cells, regardless of whether they expressed TNFα or IFNγ (e.g. cluster #10, a

203 population of CD4 T cells characterized by intermediate expression of GITR, PD-1 and
204 ICOS, Fig. 1C). In contrast, cluster #9 (depicted in black, Fig. 1B-C) contained CD44^{high}
205 IRF4^{mid} IL-2+ cells that were never found among the IFNγ-TNFα- subset of CD4 T cells.
206 Beyond these distinctions, there were two classes of cell clusters that were inversely
207 related: i) clusters enriched among IFNγ- CD4 T cells (depicted in pastel colors), and ii)
208 clusters enriched among IFNγ+ CD4 T cells (depicted in saturated colors, Fig. 1B-C).
209 Clusters enriched among IFNγ- cells were primarily CD44^{low} with limited expression of
210 notable phenotypic markers (Fig. 1C). Conversely, clusters enriched among IFNγ+
211 subsets (IFNγ+ or IFNγ+ TNFα+; clusters 8, 12 and 16) included: i) cluster #16, a
212 Tbet^{high} Lag3^{high} IRF4^{high} PD-1^{high} GITR+ CD25+ CTLA4+ ICOS+ population and ii)
213 cluster #8, a Tbet^{intermediate} IRF4^{high} IL-10^{high} GITR+ CTLA4+ PD-1+ ICOS+ population
214 (Fig. 1C). These data demonstrate that γHV68 elicits a diverse set of CD4 T cells during
215 primary infection, including the induction of an IFNγ+ IL-10+ effector CD4 T cell subset.
216
217 ***High-dimensional analysis of IL-10 expression as defined by an IL-10***
218 ***transcriptional reporter.*** Our initial analysis focused on the phenotypic diversity of
219 CD4 T cells elicited during virus infection, where we identified a prominent IL-10
220 producing effector CD4 T cell subset (cluster #8, Fig. 1C). To gain a broader
221 perspective on IL-10 expressing cells during primary virus infection, we next infected IL-
222 10 transcriptional reporter mice, in which the enhanced GFP gene is inserted 3' of the
223 endogenous Il10 gene (i.e. mice expressing the IL-10 *tiger* allele (26)). γHV68 infected
224 lungs were harvested at 6 dpi and subjected to mass cytometric analysis, where
225 samples were stained with a metal-conjugated, anti-GFP antibody to detect the IL-10

reporter (Table 2). As anticipated, γHV68 infection resulted in prominent changes in the frequency and distribution of PhenoGraph-defined clusters relative to mock infected lungs (Fig. 2A). When we analyzed the cellular distribution of the IL10gfp reporter, IL10gfp expression was detected in a fraction of cells in infected lungs, primarily within CD4 T cells (Fig. 2A).

Infection of IL-10 transcriptional reporter mice afforded a major advantage over ICCS, as it measured IL-10 mRNA expression without the need for additional pharmacologic stimuli which can alter cellular phenotype. We therefore focused on CD4 T cell phenotypes in either mock or virally-infected lungs using the PhenoGraph clustering algorithm, which identified 16 CD4 T cell clusters across mock and γHV68 infected lungs. Virally-infected lungs had an increased number of CD4 T cells relative to mock-infection, with a pronounced shift in CD4 T cell clusters (Fig. 2B) towards a prominent $CD44^{high}$ $Ki67^{high}$ $ICOS^{high}$ $PD\text{-}1^{high}$ population (Fig. 2C). Within these virally-elicited effector CD4 T cells, Lag3, Ly6C, and CD49b expression were expressed in partially overlapping cell subsets (Fig. 2C). IL10gfp expression was detected in a subset of virally-elicited effector CD4 T cells (Fig. 2C), specifically cluster #1 and #5 (Fig. 2D). IL10gfp+ CD4 T cells between these two clusters shared a conserved $CD44^{high}$ $Ki67^{high}$ $ICOS^{+}$ $PD\text{-}1^{high}$ $Lag3^{high}$ $CD49b^{mid}$ phenotype, with $Ly6C^{high}$ and $Ly6C^{low}$ subsets. These studies, using an IL-10 transcriptional reporter, demonstrate that CD4 T cells are a primary source of IL-10 expression during acute γHV68 infection and further identify a core phenotype associated with IL-10 expression within effector CD4 T cells.

γHV68 infection elicits a dominant IL10gfp expressing CD4 T cell population that differs from anti-CD3 antibody elicited IL10gfp expressing CD4 T cells. Multiple CD4 T cell subsets can produce IL-10, including type 1 regulatory CD4 T cells, a FoxP3- IL-10+ subset of CD4 T cells reported to co-express the cell surface proteins Lag3 and CD49b (22). Based on the expression of Lag3 and CD49b in IL-10 expressing CD4 T cells (Fig. 2C-D), we sought to compare how these cells compare to Tr1 cells generated by an established method. One published method to elicit Tr1 cells is the repeated injection of anti-CD3 antibody into mice, a method associated with both polyclonal T cell activation and the generation of Tr1 cells (22). In this context, Tr1 cells are found especially in the small intestine, with a lower induction of these cells in other tissues (26). To understand how virally induced IL-10+ CD4 T cells compare to IL-10+ CD4 T cells elicited following anti-CD3 antibody injection, we compared CD4 T cells from the lungs of γHV68 infected mice with CD4 T cells from the spleens of mice repeatedly injected with anti-CD3 antibody. Cells were harvested and subjected to mass cytometric analysis using a panel of 34 antibodies (Table 3). When CD4 T cells from these two conditions were subjected to the PhenoGraph algorithm, we identified 20 clusters of CD4 T cells (Fig. 3A). tSNE plots of CD4 T cells for each condition revealed largely non-overlapping cell clusters, suggesting phenotypic divergence (Fig. 3A). Across both conditions, five of twenty CD4 T cell clusters had above average expression of IL10gfp (Fig. 3B). There were large differences in the frequency of IL10gfp+ cells among CD4 T cells between conditions, with ~10% of CD4 T cells that were IL10gfp+ in the spleens of anti-CD3 antibody injected mice and ~50% of CD4 T cells that were IL10gfp+ in γHV68 infected lungs (Fig. 3C). When we analyzed the

phenotype of IL10gfp+ clusters between these two conditions, we found a significant phenotypic divergence. Within anti-CD3 antibody injected mice, the highest frequency of IL10gfp+ cells were found within a FoxP3+ regulatory T cell (Treg) cluster (Fig. 3D). In contrast, IL10gfp+ clusters that were dominant in γHV68 infection were $CD44^{high}$ $Lag3^{high}$ $PD\text{-}1^{high}$ Tbet+ and FoxP3-, suggesting they may be either Tr1 or Th1 cells (Fig. 3D). These data emphasize the multiple potential cellular sources of IL-10 that can occur with diverse stimuli, and reveal that virus infection elicits a distinct effector T cell phenotype when compared to anti-CD3 antibody injection.

IL-10 dependent regulation of γHV68 infection. To define how IL-10 regulates the distribution and phenotype of immune cell subsets during γHV68 infection we used mass cytometry to compare cellular composition and phenotype between γHV68 infected wild-type (B6) and IL-10 deficient (IL10KO) mice. This analysis focused on cellular diversity among hematopoietic (CD45+) cells within the lungs and colon, with tissues harvested from separate cohorts. Mass cytometry data were collected and subjected to the PhenoGraph algorithm for clustering analysis. This analysis identified 29 cell clusters in lungs harvested from γHV68 infected mice, with 20 cell clusters identified in the colons of γHV68 infected mice (Fig. 4A-B). Cell clusters were further defined based on canonical lineage markers, to quantify the frequencies of distinct leukocyte populations (Fig. 4C-D). When we compared cluster distribution between B6 and IL10KO mice, we found pronounced shifts in cellular distribution between B6 and IL10KO infected lungs, particularly among CD4 T cells (Fig. 4C). In contrast, colons from virally-infected mice had a very limited number of changes in cell clusters at this

time post-infection (Fig. 4D). Among the cell clusters present in infected lungs, IL10KO mice had a significantly increased frequency in two cell clusters: i) PD-1+ Lag3+ CD4 T cells (cluster #14), and ii) a small, but significant, increase in CD64+ cells (cluster #25) (Fig. 4E). Colons from infected IL10KO mice had a selective increase in the frequency of CD64+ cells characterized by a CD11b+ CD11c+ phenotype with variable CD103 expression (cluster #13) (Fig. 4F). Cluster #13 was unique among CD64+ clusters in CD11c and CD103 expression relative to other CD64+ clusters in the colon (Fig. 4F). These findings suggest that during acute γHV68 infection that IL-10 constrains the expansion and/or survival of effector CD4 T cells in the lung, and further constrains the frequency of CD64+ mononuclear phagocytic cells in both the lung and the colon.

IL-10 dependent regulation of effector CD4 T cell function during acute γHV68 infection. Next, we sought to define how IL-10 regulates CD4 T cell effector function during acute γHV68 infection, as revealed by intracellular cytokine staining analysis. We compared CD4 T cell function between γHV68 infected B6 and IL10KO mice by ICCS using mass cytometry. In contrast to the clustering analysis done in Fig. 1, CD4 T cells for both genotypes were subjected to PhenoGraph-defined clustering using 32 markers including IFNγ, TNFα and IL-10 (Table 1), identifying 16 unique clusters (Fig. 5A). CD4 T cells were predominantly $CD44^{high}$, consistent with a large effector CD4 T cell population in virally-infected lungs at this time (Fig. 5B). 7 of the 16 PhenoGraph-defined clusters showed expression of either IFNγ, TNFα and/or IL-10 (Fig. 5B), with phenotypes ranging from single expression of IFNγ+ or TNFα+, coexpression of IFNγ+ and TNFα+, and triple expression of IFNγ+ TNFα+ and IL-10+ (Fig. 5B-C). When we

317 analyzed the frequency of CD4 T cells stratified by cytokine expression, we found that
318 B6 and IL10KO mice had comparable frequencies of TNFα+ single positive and IFNγ+
319 single positive CD4 T cells (Fig. 5C-D). As anticipated, IL10KO mice had no detectable
320 IL-10+ CD4 T cells (Fig. 5C-D). B6 mice had a significantly increased frequency of
321 cytokine negative CD4 T cells (IFNγ- TNFα- IL-10-) relative to IL10KO mice (Fig. 5C-D).
322 In contrast, IL10KO mice had a significantly increased frequency of IFNγ+ TNFα+
323 effector CD4 T cells (Fig. 5C-D). While IL10KO mice had an increased frequency of
324 IFNγ+ TNFα+ CD4 T cells relative to B6 mice, both genotypes had phenotypic diversity
325 within this cytokine producing subset, including cell subsets with partially overlapping
326 expression of CTLA-4, GITR, ICOS, Lag3 and PD-1 (Fig. 5E). These data demonstrate
327 that IL-10 constrains the magnitude of highly activated IFNγ+ TNFα+ effector CD4 T
328 cells during acute γHV68 infection, a population characterized by heterogeneous
329 expression of CTLA-4, GITR, ICOS, Lag3 and PD-1.

DISCUSSION

IL-10 is a multifunctional cytokine that critically shapes the magnitude and activation status of the immune system in response to infection. In addition to its host immunomodulatory functions, IL-10 is a frequent target of viral manipulation by the herpesviruses (12, 13). Here we sought to investigate how γHV68, a small animal model of gammaherpesvirus infection, intersects with IL-10, both in terms of what cells produce IL-10 and how the overall immune response is influenced by IL-10 during acute infection. For these studies, we have focused on acute, primary infection with γHV68, seeking new insights through the use of high-dimensional mass cytometry (CyTOF) analyses.

IL-10 is known to be produced by a large number of cell types, including CD4 and CD8 T cell subsets and B cells (8). Here we make use of IL-10eGFP transcriptional reporter mice, and direct intracellular staining for IL-10 protein, to identify CD4 T cells as a primary source of IL-10 production during acute γHV68 infection in the lung. IL-10+ CD4 T cells elicited during viral infection were associated with a highly activated effector phenotype, characterized by high expression of CD44 with co-expression of the cytokines IFNγ and TNFα. IL10gfp+ CD4 T cells were proliferating and characterized by expression of PD-1, Lag3, ICOS, CD49b with variable expression of Ly6C. By querying these cellular phenotypes using mass cytometry, we have further analyzed IL10gfp expression across a wide range of leukocyte subsets. These studies demonstrated focused expression of IL-10 within CD4 T cells in the infected lung with minimal IL-10 expression in other cell subsets at this time.

352 The expression of IL-10 within this highly activated effector CD4 T cells raises
353 the question of what effector subset(s) express IL-10 in this context. Our data
354 demonstrate that FoxP3+ Tregs are not a prominent source of IL-10 during acute γHV68
355 infection in the lung. Instead, IL-10+ CD4 T cells appear to be either: 1) type 1
356 regulatory T cells, an IL-10 expressing, FoxP3 negative subset of CD4 T cells frequently
357 characterized by co-expression of CD49b and Lag3 (22), or 2) an IL-10 expressing Th1
358 subset (27-29). While these cells co-express CD49b and Lag3, a proposed marker of
359 Tr1 cells (22), recent studies have emphasized that co-expression of CD49b and Lag3
360 is not a definitive marker of Tr1 cells (30, 31). Conversely, IFNγ+ Th1 cells have been
361 reported to express IL-10 in a variety of settings (32), and γHV68 induced IL-10+
362 effectors express the canonical Th1 transcription factor Tbet. Despite these
363 observations, at this time there remains no definitive marker that discriminates between
364 Tr1 and Th1 cells. Alternatively, these IFNγ+ IL-10+ expressing cells may represent a
365 distinct effector CD4 T cell subset (33). Recently, Eomesodermin was identified as a
366 transcriptional regulator for IL-10+ effector CD4 T cells, in both Tr1 cells (30) and a
367 potentially distinct IFNγ+ IL-10+ effector CD4 T cell (34). Whether IL-10+ CD4 T cells
368 elicited during γHV68 infection express, and require, Eomesodermin remains to be
369 tested.

370 IL-10 regulates its effects through signals transduced by the heterodimeric IL-10
371 receptor, targeting both myeloid and non-myeloid cells (9). High-dimensional analysis of
372 the immune response after γHV68 infection identified a wide spectrum of cells in
373 infected lung and colon, a phenotypic diversity readily characterized through use of the
374 PhenoGraph clustering algorithm and visualized by the tSNE data dimensionality

375 method. When we compared cellular and phenotypic diversity between B6 and IL10KO
376 mice, we found a pronounced increase in the frequency of a PD-1+ Lag3+ CD4 T cell
377 subset and an exaggerated induction of IFNγ+ TNFα+ effector CD4 T cells. We further
378 found evidence for changes in CD64+ populations in both the infected lung and colon.
379 While IL-10 may directly regulate effector CD4 T cell function (35, 36), CD4 T cell
380 differentiation and effector function may also occur due to altered myeloid function(s) (8,
381 10, 37, 38). Future studies using targeted disruption of IL-10 signaling in myeloid cells
382 (e.g. macrophages, dendritic cells) and T cells will be required to determine whether IL-
383 10 directly or indirectly modulates effector CD4 T cell differentiation during γHV68
384 infection. Regardless of the molecular basis of this phenoype, the increased frequency
385 of PD-1+ Lag3+ effector CD4 T cells in IL-10 deficient mice suggests that co-inhibitory
386 receptor expression may function as a compensatory mechanism to constrain
387 pathogenic CD4 T cell function in the absence of IL-10.

388 Beyond insights on IL-10 dependent regulation during γHV68 infection, these
389 studies demonstrate the power of high-dimensional approaches such as mass
390 cytometry to investigate the regulation of the immune response at a global level. By
391 applying mass cytometry to CD4 T cells, our studies provide direct evidence for
392 extensive phenotypic diversity of antiviral effector CD4 T cells elicited during primary
393 viral infection. We anticipate that future studies, integrating mass cytometry with host
394 and viral genetics, will afford new insights into the underpinnings of antiviral CD4 T cell
395 function from a high-dimensional perspective.

FIGURE LEGENDS

Figure 1. High-dimensional analysis of CD4 T cells elicited during primary γHV68 infection. Mass cytometric analysis of cells recovered from the lungs of γHV68 infected C57BL/6J (B6) mice at 9 dpi, subjected to intracellular cytokine staining (ICCS) analysis, using a 35 antibody panel (Table 1). Data were gated on viable CD4 T cells, defined as ^{191}Ir+ ^{193}Ir+ ^{195}Pt- ^{152}CD3ε+ ^{172}CD4+ ^{174}MHC II- events, where numbers indicate isotopic mass for each measured parameter. (A) Analysis of IFNγ and TNFα production from CD4 T cells subjected to pharmacologic stimulation with PMA and ionomycin. The mean ± SEM for each population is identified in each quadrant. Events in each quadrant were further analyzed using the PhenoGraph algorithm and plotted using the tSNE dimensionality reduction algorithm. Events were imported into PhenoGraph and clustered on 8,320 events total and 30 markers (clustering parameters identified in Table 1). In total 16 clusters were identified, with clusters colored by cluster ID and displayed on tSNE plots. (B) Distribution of PhenoGraph-defined clusters within CD4 T cells, stratified by expression of IFNγ and TNFα. Each pie chart is subdivided into clusters that are equally represented in IFNγ- and IFNγ+ CD4 T cells (shades of gray), clusters that are enriched in IFNγ- CD4 T cells (pastel colors), clusters that are enriched only in cytokine producing CD4 T cells (black), and clusters that are enriched in IFNγ+ CD4 T cells (saturated colors) as defined in the key. Right panel shows events depicted using tSNE, where each cluster is colored according to the cytokine profile subsets (see key). (C) Phenotypic marker expression (in columns) of PhenoGraph-defined clusters (in rows), stratified by their enrichment as a function of cytokine profile.

Clusters are stratified as in panel B. Data are from virally infected B6 lungs (n=4 mice) harvested 9 dpi, with cells stimulated with PMA and ionomycin for five hours prior to antibody staining.

Figure 2. High-dimensional analysis of IL10gfp expression during acute γHV68 infection in the lung. Mass cytometric analysis of cells recovered from the lungs of γHV68 infected IL10gfp mice at 6 dpi. Files were normalized, with events gated on (A) total viable, single cells (defined as ^{191}Ir+ ^{193}Ir+ ^{195}Pt-) or (B-D) viable, CD4+ T cells (defined as ^{191}Ir+ ^{193}Ir+ ^{195}Pt- ^{152}CD3ε+ ^{172}CD4+ ^{174}MHC II-) prior to analysis, where numbers indicate isotopic mass for each measured parameter. (A) PhenoGraph analysis of cellular phenotypes in mock and virally-infected lung (28,924 events total), clustered based on 29 markers (Table 2), identified 34 unique clusters, with cluster phenotype defined according to the indicated lineage markers. The “CD45+” cluster was defined by its expression of CD45+ and absence of other lineage defining markers. The right panel of A shows all viable, singlet events from mock- and virally-infected lungs, with events colored according to IL10gfp expression. The green boundary line defines CD4+ T cells. (B) Mass cytometric analysis and PhenoGraph-based cell clustering of CD4+ T cells (5,464 events total, clustered based on 26 markers, excluding CD3, CD4, and MHC II, Table 2). In total 16 unique clusters were identified, visualized on a tSNE plot (left). The number and frequency of CD4 T cell clusters is shown in the right panel, with pie charts sized proportionally to the relative cell number of CD4 T cells in mock or virus infected lung. (C) Phenotypic analysis of CD4 T cells, with events predominantly in mock infection denoted with a gray boundary and events predominantly in virus

infection denoted with a red boundary. Data depict CD4 T cells plotted according to tSNE1 and tSNE2, as in panel B, with individual plots depicting relative protein expression for the identified marker portrayed by color intensity, with range of expression indicated on the bottom of each panel. Panels are ordered based on the frequency of positive events. (D) Summary of CD4 T cell clusters (in columns) that differ between mock and γHV68 infected lungs, with protein expression denoted in rows (gray shading scaled relative to expression level). Data are from the lungs of a mock- or γHV68-infected mouse harvested at 6 dpi, with panel D quantifying the frequency of events in each cluster as a percentage of CD4+ T cells.

Figure 3. γHV68 infection elicits a dominant IL10gfp expressing CD4 T cell population that differs relative to IL10gfp expressing CD4 T cells in anti-CD3 antibody injected mice. Mass cytometric analysis of cells recovered from IL10gfp mice, comparing CD4 T cell phenotypes between the spleens of anti-CD3 antibody injected mice with the lungs of γHV68 infected mice harvested at 6 dpi. Files were normalized and gated on viable, CD4+ T cells (defined as ^{191}Ir+ ^{193}Ir+ ^{195}Pt- ^{152}CD3ε+ ^{172}CD4+ ^{209}MHC II-) prior to analysis, where numbers indicate isotopic mass for each measured parameter. (A) PhenoGraph analysis of CD4 T cells, comparing anti-CD3 antibody injected versus γHV68 infected samples (75,483 events total, clustered on 33 markers, excluding CD3, CD4, and MHC II, Table 3), identified 20 unique clusters, each denoted with a distinct color. (B) PhenoGraph-defined CD4 T cell clusters were ranked based on IL10gfp expression, with 5 clusters having higher than average IL10gfp expression identified in red text. Figure insets depict all events from panel A, colored

according to (left panel) IL10gfp expression, or (right panel) cluster ID for 5 IL10gfp+ clusters. (C) The frequencies of CD4 T cell clusters are shown for both conditions, with focused analysis on the distribution of IL10gfp+ clusters identified by shaded gray extensions and pie charts on either side. Pie charts denote the frequencies of IL10gfp+ events in each condition, with pie charts sized according to the relative number of IL10gfp+ events present in each condition. (D) Comparison of median protein expression within IL10gfp+ CD4 T cell clusters in either anti-CD3 antibody injected spleens and/or γHV68 infected lungs. Cellular markers are ordered from greatest to least range in median expression between clusters. Data are from IL10gfp mice, using either spleens from mice that were injected with an anti-CD3 antibody (injected with antibody at 0 and 46 hours, with harvest at 50 hours, n=4 mice) or lungs from γHV68 infected (n=5 mice) harvested at 6 dpi.

Figure 4. High dimensional analysis of IL-10 dependent regulation of the antiviral response in the lung and the colon. Mass cytometric analysis of cells recovered the lungs (A,C,E) or colons (B,D,F) of γHV68 infected B6 or IL10KO mice harvested at 9 dpi. Files were normalized and gated on viable, single CD45+ cells (defined as ^{191}Ir+ ^{193}Ir+ ^{195}Pt- ^{89}CD45+) prior to analysis, where numbers indicate isotopic mass for each measured parameter. (A, B) PhenoGraph analysis of CD45+ cells from (A) lungs or (B) colons of γHV68 infected B6 or IL10KO mice. Clustering was done on 4,344 events per file (34,752 total), with clustering in the lung based on 34 markers (29 clusters identified, Table 4A) and clustering in the colon based on 36 markers (20 clusters identified, Table 4B); lungs and colons were harvested from separate cohorts. PhenoGraph-defined

clusters are colored according to cluster ID. (C,D) Definition of cellular phenotypes across PhenoGraph-defined clusters, according to the indicated lineage markers, with distinct cell types given unique colors. “CD45+ MHC II+” and “CD45+ MHC II-” clusters were defined by exclusion from other phenotypes. (E,F) Identification of clusters with statistically significant differences in frequency between B6 and IL10KO infected (E) lungs and (F) colons, showing cluster frequencies (left panel) and expression for the identified parameters within the identified cluster (right panel). In the right panel of E, plotted events are CD4+ T cells identified in panel C. In the right panel of F, plotted events are the dominant CD64+ cell clusters identified in panel D. Parameters with a different maximum scale value between B6 and IL10KO are identified by italicized text and an asterisk. Data are from γHV68 infected B6 and IL10KO lungs (n=4 mice per genotype) and colons (n=4 mice per genotype) harvested 9 dpi. Data depict mean ± SEM with individual symbols indicating values from independent samples. All samples were analyzed for statistical significance using unpaired t tests, corrected for multiple comparisons using the Holm-Sidak method, with statistical significance denoted as * $p<0.05$, ** $p<0.01$, ***$p<0.001$.

Figure 5. High-dimensional analysis of effector CD4 T cell function following γHV68 infection in B6 and IL10KO mice. Mass cytometric analysis of cells recovered the lungs of γHV68 infected B6 or IL10KO mice harvested at 9 dpi, with cells subjected to pharmacologic stimulation for intracellular cytokine staining analysis (ICCS), using a 35 antibody panel (Table 1). Files were normalized, with data gated on viable CD4 T cells, defined as ^{191}Ir+ ^{193}Ir+ ^{195}Pt- ^{152}CD3ε+ ^{172}CD4+ ^{174}MHC II- events, where numbers

511 indicate isotopic mass for each measured parameter. (A) CD4 T cells were imported
512 into PhenoGraph and clustered on 33,022 total events (3,669 events from each file) and
513 32 markers (excluding CD3, CD4, and MHC II, Table 1), identifying 16 unique clusters
514 portrayed on a tSNE plot. (B) All events from panel A are colored by CD44, IFNγ, TNFα,
515 and IL-10 expression. (C) Events from panel A colored based on their cytokine profile,
516 stratified based on IFNγ, TNFα, and IL-10 expression. (D) Frequency of CD4 T cells in
517 virally-infected B6 and IL10KO mice. (E) Comparison of CTLA-4, GITR, ICOS, Lag3,
518 and PD-1 expression across CD4 T cells from B6 (top row) or IL10KO (bottom row)
519 mice, where IFNγ+ TNFα+ CD4 T cells were identified by a green boundary line.
520 Parameters with a different maximum scale value between B6 and IL10KO are
521 identified by italicized text and an asterisk. Data from virally infected lungs of B6 (n=4)
522 and IL10KO (n= 5) mice harvested 9 dpi, with cells were further stimulated with PMA
523 and ionomycin for five hours after harvesting for ICCS. Data for B6 mice were also
524 included in Figure 1, subjected to different clustering parameters (as outlined in Table
525 1). Data show mean ± SEM with individual symbols denoting individual mice, with
526 statistical analysis done by unpaired t test, corrected for multiple comparisons using the
527 Holm-Sidak method. Statistical significance denoted by **, $p<0.01$ and ***, $p<0.001$. ns,
528 not significant.

ACKNOWLEDGEMENTS

The authors acknowledge Melissa Ledezma for technical assistance, Kristina Terrell, Christine Childs, and Karen Helm for technical support for CyTOF studies including machine operation and management of the CU CyTOF antibody bank, and the CyTOF User Group at the University of Colorado Anschutz Medical Campus for their ongoing collaboration and insights.

DISCLOSURES

The authors have no financial conflicts of interest.

REFERENCES

1. Longnecker, R. M., Kieff, E., Cohen, J.I. 2013. Epstein-Barr Virus. In *Fields Virology*, 6th ed.

2. Dittmer, D. P., and B. Damania. 2016. Kaposi sarcoma-associated herpesvirus: immunobiology, oncogenesis, and therapy. *J Clin Invest* 126: 3165-3175.

3. Barton, E., P. Mandal, and S. H. Speck. 2011. Pathogenesis and host control of gammaherpesviruses: lessons from the mouse. *Annu Rev Immunol* 29: 351-397.

4. Cesarman, E. 2014. Gammaherpesviruses and lymphoproliferative disorders. *Annu Rev Pathol* 9: 349-372.

5. Mariggio, G., S. Koch, and T. F. Schulz. 2017. Kaposi sarcoma herpesvirus pathogenesis. *Philos Trans R Soc Lond B Biol Sci* 372.

6. Ressing, M. E., M. van Gent, A. M. Gram, M. J. Hooykaas, S. J. Piersma, and E. J. Wiertz. 2015. Immune Evasion by Epstein-Barr Virus. *Curr Top Microbiol Immunol* 391: 355-381.

7. Hu, Z., and E. J. Usherwood. 2014. Immune escape of gamma-herpesviruses from adaptive immunity. *Rev Med Virol* 24: 365-378.

8. Saraiva, M., and A. O'Garra. 2010. The regulation of IL-10 production by immune cells. *Nat Rev Immunol* 10: 170-181.

9. Ouyang, W., S. Rutz, N. K. Crellin, P. A. Valdez, and S. G. Hymowitz. 2011. Regulation and functions of the IL-10 family of cytokines in inflammation and disease. *Annu Rev Immunol* 29: 71-109.

10. Rojas, J. M., M. Avia, V. Martin, and N. Sevilla. 2017. IL-10: A Multifunctional Cytokine in Viral Infections. *J Immunol Res* 2017: 6104054.

562 11. Hsu, D. H., R. de Waal Malefyt, D. F. Fiorentino, M. N. Dang, P. Vieira, J. de
563 Vries, H. Spits, T. R. Mosmann, and K. W. Moore. 1990. Expression of
564 interleukin-10 activity by Epstein-Barr virus protein BCRF1. *Science* 250: 830-
565 832.
566 12. Moore, K. W., P. Vieira, D. F. Fiorentino, M. L. Trounstine, T. A. Khan, and T. R.
567 Mosmann. 1990. Homology of cytokine synthesis inhibitory factor (IL-10) to the
568 Epstein-Barr virus gene BCRFI. *Science* 248: 1230-1234.
569 13. Siegel, A. M., J. H. Herskowitz, and S. H. Speck. 2008. The MHV68 M2 protein
570 drives IL-10 dependent B cell proliferation and differentiation. *PLoS Pathog* 4:
571 e1000039.
572 14. Peacock, J. W., and K. L. Bost. 2001. Murine gammaherpesvirus-68-induced
573 interleukin-10 increases viral burden, but limits virus-induced splenomegaly and
574 leukocytosis. *Immunology* 104: 109-117.
575 15. Nelson, D. A., C. C. Petty, and K. L. Bost. 2009. Infection with murine
576 gammaherpesvirus 68 exacerbates inflammatory bowel disease in IL-10-deficient
577 mice. *Inflamm Res* 58: 881-889.
578 16. Molloy, M. J., W. Zhang, and E. J. Usherwood. 2011. Suppressive CD8+ T cells
579 arise in the absence of CD4 help and compromise control of persistent virus. *J*
580 *Immunol* 186: 6218-6226.
581 17. Spitzer, M. H., and G. P. Nolan. 2016. Mass Cytometry: Single Cells, Many
582 Features. *Cell* 165: 780-791.

583 18. Virgin, H. W. t., P. Latreille, P. Wamsley, K. Hallsworth, K. E. Weck, A. J. Dal
584 Canto, and S. H. Speck. 1997. Complete sequence and genomic analysis of
585 murine gammaherpesvirus 68. *J Virol* 71: 5894-5904.
586 19. Adler, H., M. Messerle, M. Wagner, and U. H. Koszinowski. 2000. Cloning and
587 mutagenesis of the murine gammaherpesvirus 68 genome as an infectious
588 bacterial artificial chromosome. *J Virol* 74: 6964-6974.
589 20. Nealy, M. S., C. B. Coleman, H. Li, and S. A. Tibbetts. 2010. Use of a virus-
590 encoded enzymatic marker reveals that a stable fraction of memory B cells
591 expresses latency-associated nuclear antigen throughout chronic
592 gammaherpesvirus infection. *J Virol* 84: 7523-7534.
593 21. Diebel, K. W., L. M. Oko, E. M. Medina, B. F. Niemeyer, C. J. Warren, D. J.
594 Claypool, S. A. Tibbetts, C. D. Cool, E. T. Clambey, and L. F. van Dyk. 2015.
595 Gammaherpesvirus small noncoding RNAs are bifunctional elements that
596 regulate infection and contribute to virulence in vivo. *MBio* 6: e01670-01614.
597 22. Gagliani, N., C. F. Magnani, S. Huber, M. E. Gianolini, M. Pala, P. Licona-Limon,
598 B. Guo, D. R. Herbert, A. Bulfone, F. Trentini, C. Di Serio, R. Bacchetta, M.
599 Andreani, L. Brockmann, S. Gregori, R. A. Flavell, and M. G. Roncarolo. 2013.
600 Coexpression of CD49b and LAG-3 identifies human and mouse T regulatory
601 type 1 cells. *Nat Med* 19: 739-746.
602 23. Kimball, A. K., L. M. Oko, B. L. Bullock, R. A. Nemenoff, L. F. van Dyk, and E. T.
603 Clambey. 2018. A Beginner's Guide to Analyzing and Visualizing Mass
604 Cytometry Data. *J Immunol* 200: 3-22.

605 24. Hu, Z., M. A. Blackman, K. M. Kaye, and E. J. Usherwood. 2015. Functional
606 heterogeneity in the CD4+ T cell response to murine gamma-herpesvirus 68. *J*
607 *Immunol* 194: 2746-2756.
608 25. Levine, J. H., E. F. Simonds, S. C. Bendall, K. L. Davis, A. D. Amir el, M. D.
609 Tadmor, O. Litvin, H. G. Fienberg, A. Jager, E. R. Zunder, R. Finck, A. L.
610 Gedman, I. Radtke, J. R. Downing, D. Pe'er, and G. P. Nolan. 2015. Data-Driven
611 Phenotypic Dissection of AML Reveals Progenitor-like Cells that Correlate with
612 Prognosis. *Cell* 162: 184-197.
613 26. Kamanaka, M., S. T. Kim, Y. Y. Wan, F. S. Sutterwala, M. Lara-Tejero, J. E.
614 Galan, E. Harhaj, and R. A. Flavell. 2006. Expression of interleukin-10 in
615 intestinal lymphocytes detected by an interleukin-10 reporter knockin tiger
616 mouse. *Immunity* 25: 941-952.
617 27. Sun, J., R. Madan, C. L. Karp, and T. J. Braciale. 2009. Effector T cells control
618 lung inflammation during acute influenza virus infection by producing IL-10. *Nat*
619 *Med* 15: 277-284.
620 28. Weiss, K. A., A. F. Christiaansen, R. B. Fulton, D. K. Meyerholz, and S. M.
621 Varga. 2011. Multiple CD4+ T cell subsets produce immunomodulatory IL-10
622 during respiratory syncytial virus infection. *J Immunol* 187: 3145-3154.
623 29. Parish, I. A., H. D. Marshall, M. M. Staron, P. A. Lang, A. Brustle, J. H. Chen, W.
624 Cui, Y. C. Tsui, C. Perry, B. J. Laidlaw, P. S. Ohashi, C. T. Weaver, and S. M.
625 Kaech. 2014. Chronic viral infection promotes sustained Th1-derived
626 immunoregulatory IL-10 via BLIMP-1. *J Clin Invest* 124: 3455-3468.

627 30. Zhang, P., J. S. Lee, K. H. Gartlan, I. S. Schuster, I. Comerford, A. Varelias, M.
628 A. Ullah, S. Vuckovic, M. Koyama, R. D. Kuns, K. R. Locke, K. J. Beckett, S. D.
629 Olver, L. D. Samson, M. Montes de Oca, F. de Labastida Rivera, A. D. Clouston,
630 G. T. Belz, B. R. Blazar, K. P. MacDonald, S. R. McColl, R. Thomas, C. R.
631 Engwerda, M. A. Degli-Esposti, A. Kallies, S. K. Tey, and G. R. Hill. 2017.
632 Eomesodermin promotes the development of type 1 regulatory T (TR1) cells. *Sci*
633 *Immunol* 2.
634 31. Huang, W., S. Solouki, C. Carter, S. G. Zheng, and A. August. 2018. Beyond
635 Type 1 Regulatory T Cells: Co-expression of LAG3 and CD49b in IL-10-
636 Producing T Cell Lineages. *Front Immunol* 9: 2625.
637 32. Jankovic, D., D. G. Kugler, and A. Sher. 2010. IL-10 production by CD4+ effector
638 T cells: a mechanism for self-regulation. *Mucosal Immunol* 3: 239-246.
639 33. Haringer, B., L. Lozza, B. Steckel, and J. Geginat. 2009. Identification and
640 characterization of IL-10/IFN-gamma-producing effector-like T cells with
641 regulatory function in human blood. *J Exp Med* 206: 1009-1017.
642 34. Gruarin, P., S. Maglie, M. De Simone, B. Haringer, C. Vasco, V. Ranzani, R.
643 Bosotti, J. S. Noddings, P. Larghi, F. Facciotti, M. L. Sarnicola, M. Martinovic, M.
644 Crosti, M. Moro, R. L. Rossi, M. E. Bernardo, F. Caprioli, F. Locatelli, G. Rossetti,
645 S. Abrignani, M. Pagani, and J. Geginat. 2018. Eomesodermin controls a unique
646 differentiation program in human IL-10 and IFN-gamma coproducing regulatory T
647 cells. *Eur J Immunol*.
648 35. Sun, J., A. Cardani, A. K. Sharma, V. E. Laubach, R. S. Jack, W. Muller, and T.
649 J. Braciale. 2011. Autocrine regulation of pulmonary inflammation by effector T-

650 cell derived IL-10 during infection with respiratory syncytial virus. *PLoS Pathog* 7:
651 e1002173.
652 36. Brockmann, L., N. Gagliani, B. Steglich, A. D. Giannou, J. Kempski, P. Pelczar,
653 M. Geffken, B. Mfarrej, F. Huber, J. Herkel, Y. Y. Wan, E. Esplugues, M.
654 Battaglia, C. F. Krebs, R. A. Flavell, and S. Huber. 2017. IL-10 Receptor
655 Signaling Is Essential for TR1 Cell Function In Vivo. *J Immunol* 198: 1130-1141.
656 37. Mittal, S. K., and P. A. Roche. 2015. Suppression of antigen presentation by IL-
657 10. *Curr Opin Immunol* 34: 22-27.
658 38. Ip, W. K. E., N. Hoshi, D. S. Shouval, S. Snapper, and R. Medzhitov. 2017. Anti-
659 inflammatory effect of IL-10 mediated by metabolic reprogramming of
660 macrophages. *Science* 356: 513-519.
661

CD4 T cells (191+ 193+ 195 CD3+ CD4+ MHCII- events), stimulated for ICOS

A.

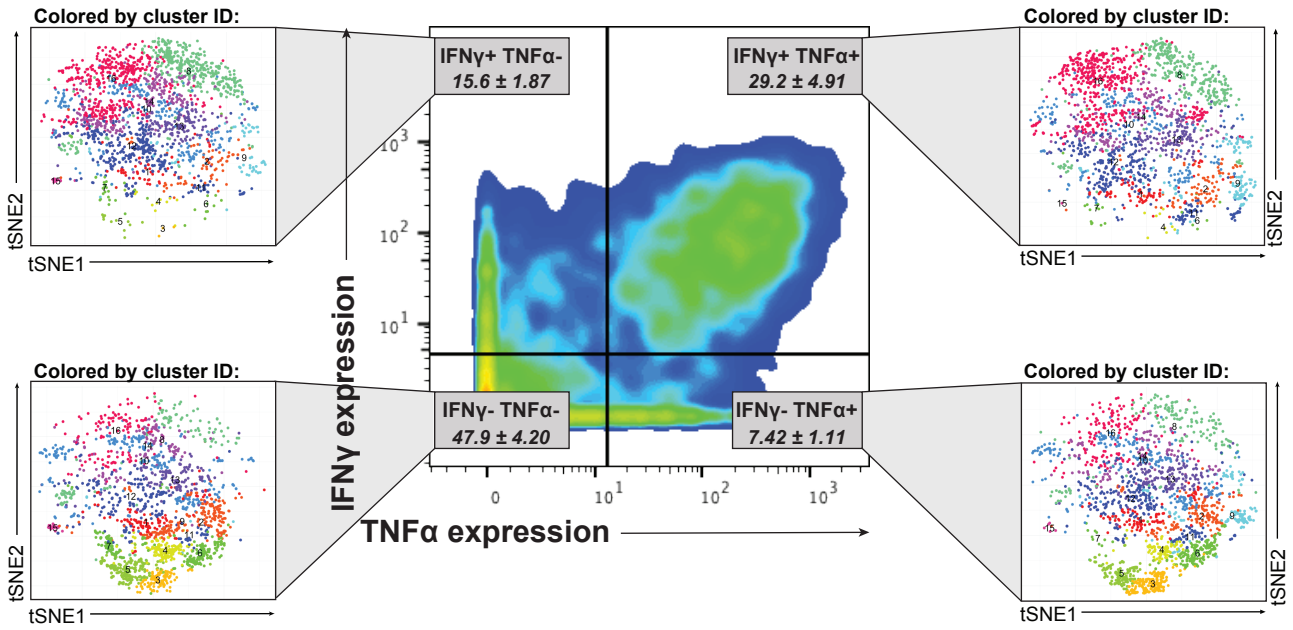

B.

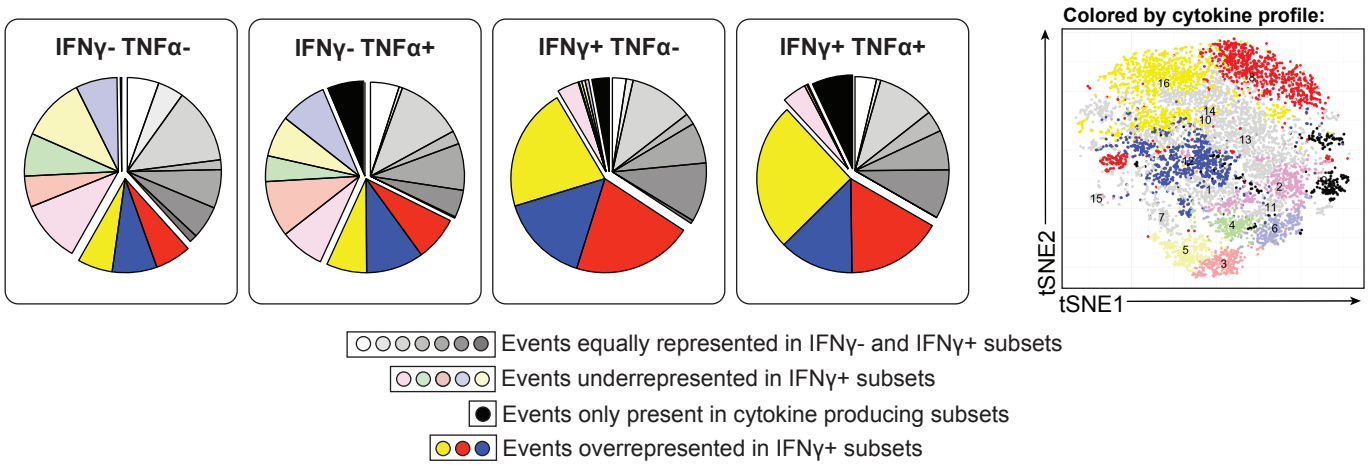

C.

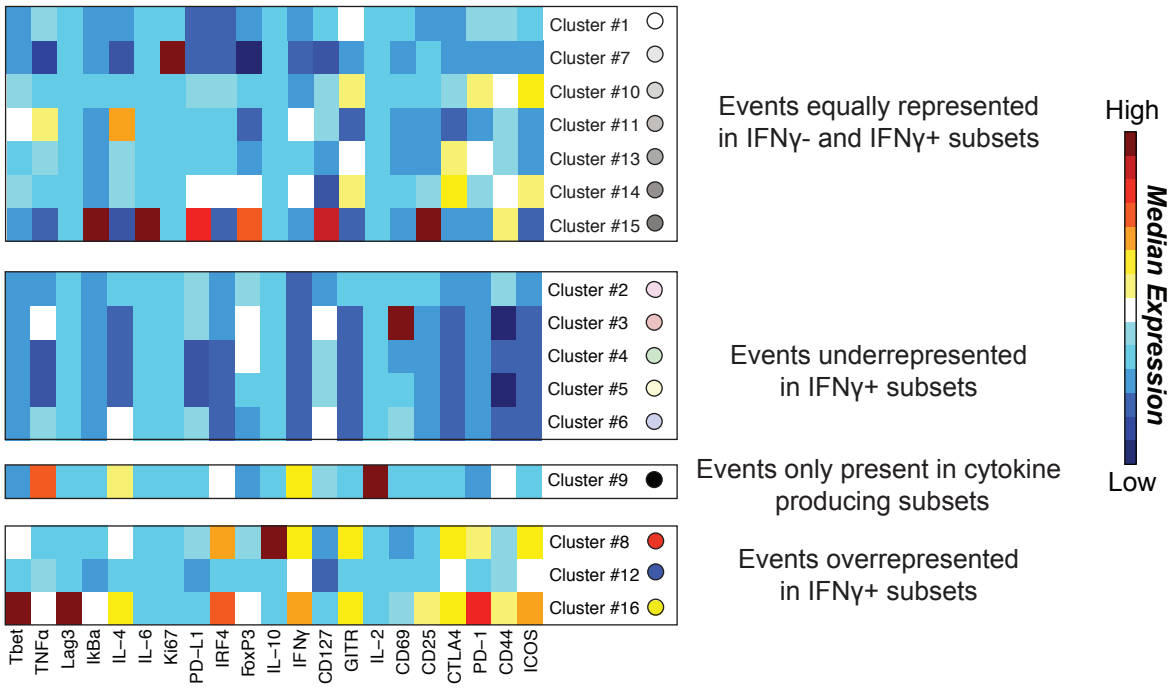

Kimball et al
Figure 1

Live, Singlet Events (191+ 193+ 195- events)

A.

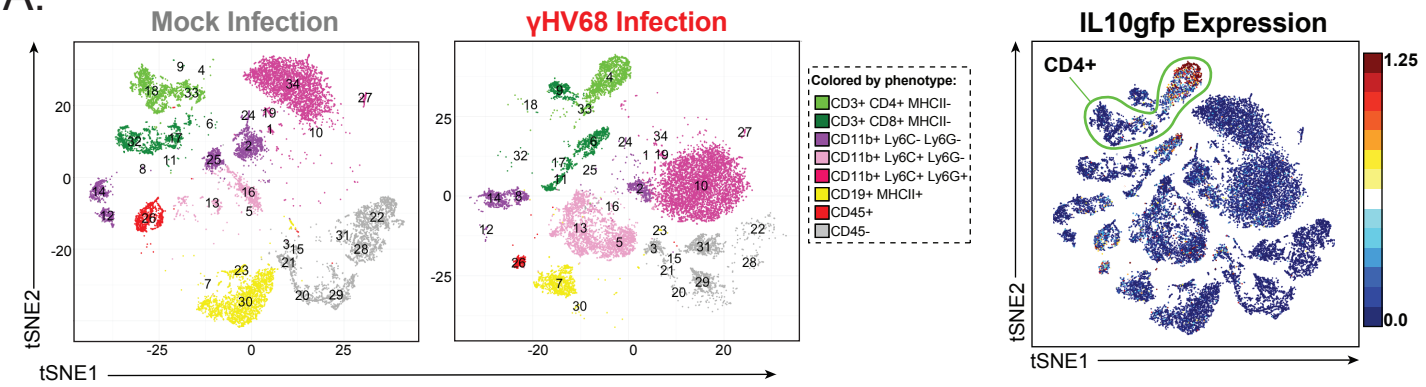

CD4 T cells (191+ 193+ 195- CD3+ CD4+ MHCII- events)

B.

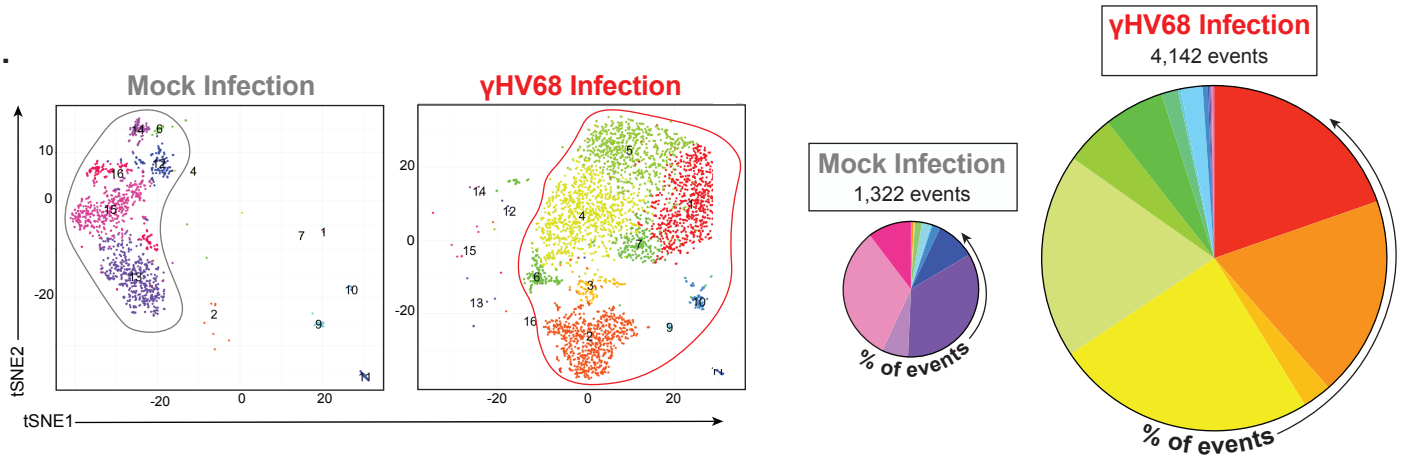

C.

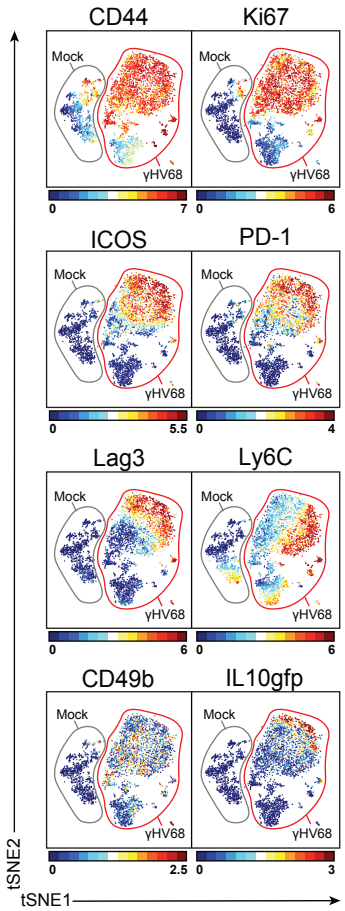

D.

Enriched in mock infection				Enriched in γHV68 infection				
Cluster ID								
#12	#13	#14	#15	#1	#2	#4	#5	
Hi	Lo	Hi	Lo	Hi	Mid	Hi	Hi	**CD44**
Hi	Lo	Lo	Lo	Hi	Lo	Hi	Hi	**Ki67**
Lo	Lo	Lo	Lo	Mid	Lo	Mid	Hi	**ICOS**
Lo	Lo	Lo	Lo	Hi	Lo	Mid	Hi	**PD-1**
Lo	Lo	Lo	Lo	Hi	Lo	Lo	Hi	**Lag3**
Lo	Mid	Lo	Lo	Hi	Mid	Mid	Lo	**Ly6C**
Lo	Lo	Mid	Lo	Mid	Lo	Mid	Mid	**CD49b**
-	-	-	-	+/-	-	-	+/-	**IL10gfp**
9.4%	34.2%	6.3%	32.7%	0.1%	0.6%	0.3%	0.0%	**% of mock**
0.1%	0.1%	0.1%	0.1%	19.7%	18.8%	24.5%	19.2%	**% of infected**

Protein Markers

Kimball et al
Figure 2

CD4 T cells (191+ 193+ 195- CD3+ CD4+ MHCII- events)

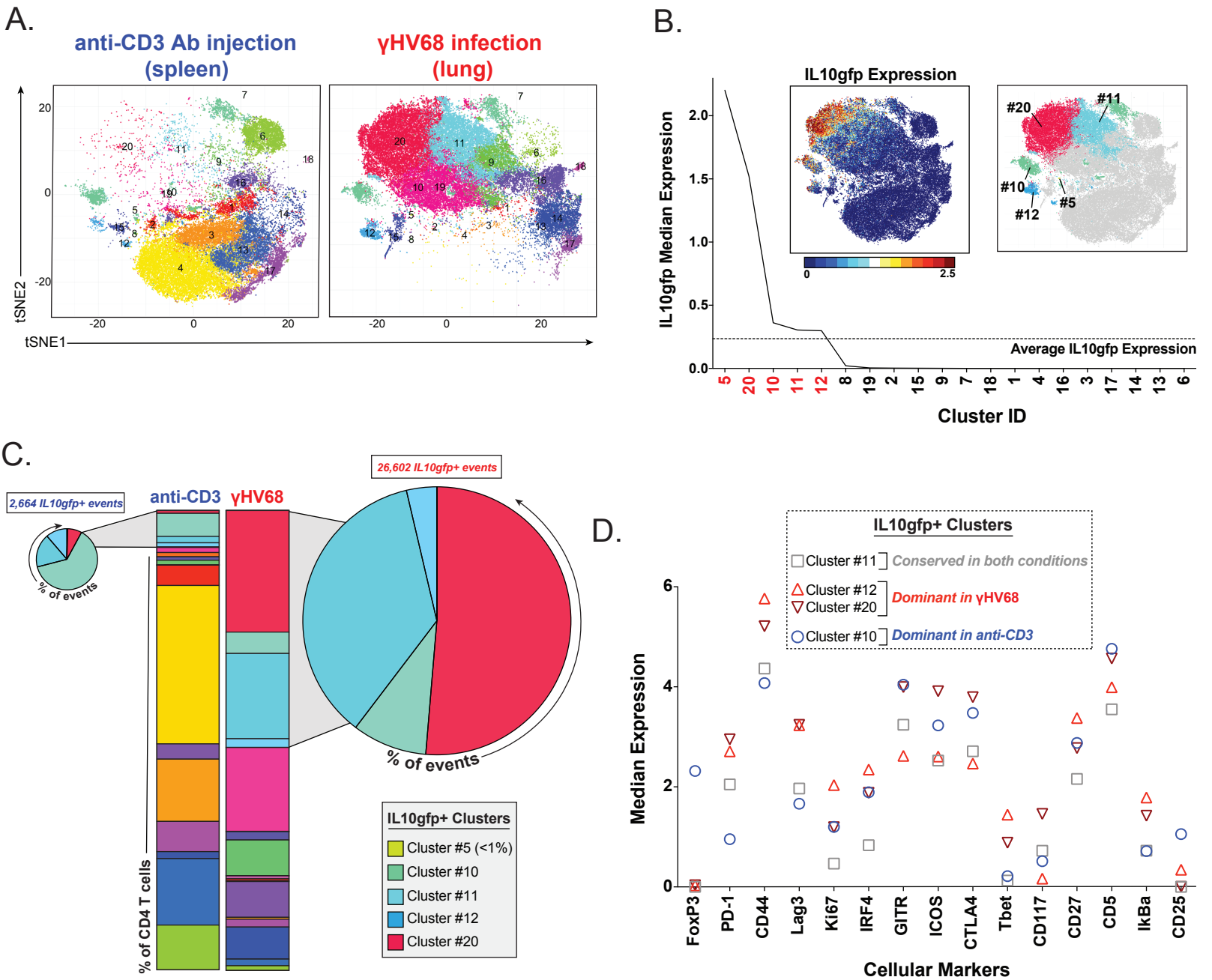

Kimball et al
Figure 3

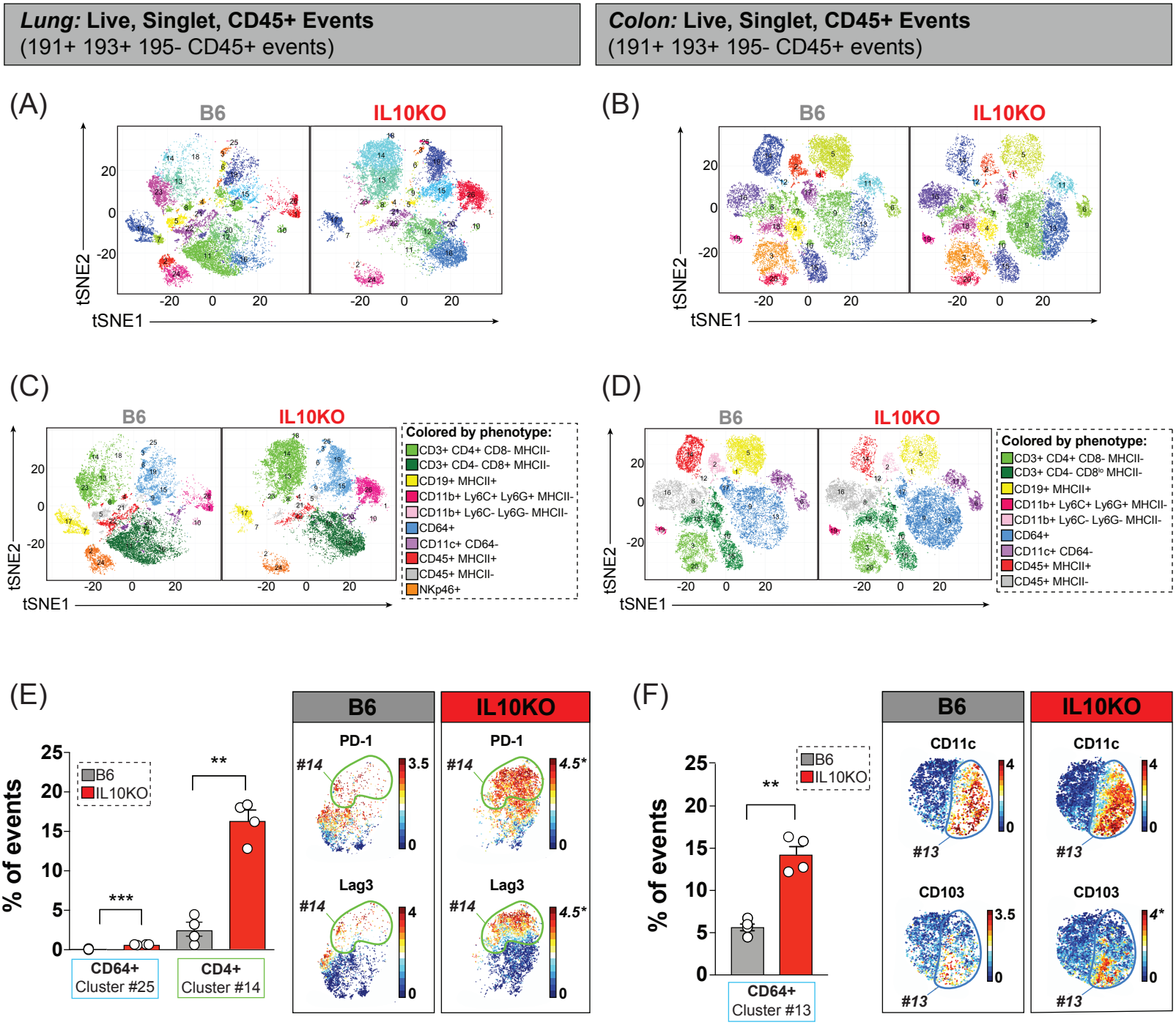

Kimball et al
Figure 4

CD4 T cells (191+ 193+ 195- CD3+ CD4+ MHCII- events), stimulated for ICCS

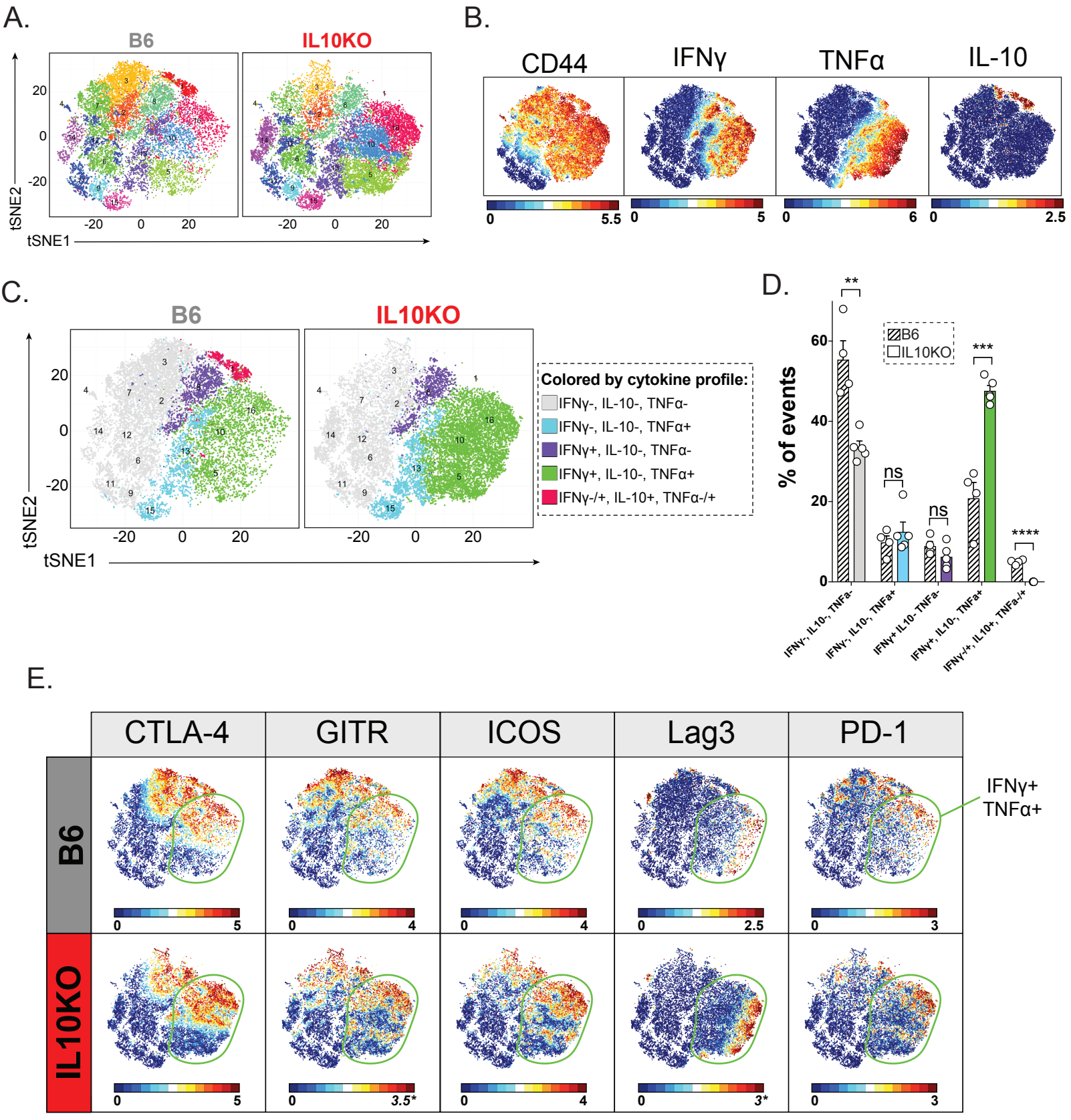

Kimball et al
Figure 5

Table 1. Antibody conjugates used for the analysis in Figure 1 and 5.

Tag	Target	Ab Clone	Surface/Intracellular	Clustering*
^{89}Y	CD45	30-F11	Surface	Yes
^{141}Pr	Gr1 (Ly6C/Ly6G)	RB6-8C5	Surface	Yes
^{142}Nd	CD11c	N418	Surface	Yes
^{143}Nd	GITR (CD357)	DTA1	Surface	Yes
^{144}Nd	IL-2	JES6-5H4	Intracellular	Yes
^{145}Nd	CD69	H1.2F3	Surface	Yes
^{146}Nd	CD8α	53-6.7	Surface	Yes
^{148}Nd	CD11b	M1/70	Surface	Yes
^{149}Sm	CD19	6D5	Surface	Yes
^{150}Nd	CD25	3C7	Surface	Yes
^{151}Eu	CD64	X54-5/7.1	Surface	Yes
^{152}Sm	CD3ε	145-2C11	Surface	No
^{153}Eu	PD-L1 (CD274)	10F.9G2	Surface	Yes
^{154}Sm	CTLA4 (CD152)	UC10-4B9	Intracellular	Yes
^{155}Gd	IRF4	3E4	Intracellular	Yes
^{156}Gd	FoxP3-PE / anti-PE	FJK-16s (Thermo Fisher) / PE001 (anti-PE)	Intracellular/Secondary	Yes
^{158}Gd	IL-10	JES5-16E3	Intracellular	Yes
^{159}Tb	PD-1 (CD279)	RMP1-30	Surface	Yes
^{160}Gd	GMCSF-FITC / anti-FITC	MP1-22E9 (Pharmingen) / FIT-22 (anti-FITC)	Intracellular/Secondary	Yes
^{161}Dy	Tbet	4B10	Intracellular	Yes
^{162}Dy	TNFα	MP6-XT22	Intracellular	No (Fig. 1) Yes (Fig. 5)
^{163}Dy	Lag3-APC / anti-APC	C9B7W (Biolegend) / APC003 (anti-APC)	Surface/Secondary	Yes
^{164}Dy	IkBα	L35A5	Intracellular	Yes
^{165}Ho	IFNγ	XMG1.2	Intracellular	No (Fig. 1) Yes (Fig. 5)
^{166}Er	IL-4	11B11	Intracellular	Yes
^{167}Er	IL-6	MP5-20F3	Intracellular	Yes
^{168}Er	Ki-67	B56	Intracellular	Yes
^{169}Tm	Ly-6A/E (Sca-1)	D7	Surface	Yes
^{170}Er	NK1.1 (CD161)	PK136	Surface	Yes
^{171}Yb	CD44	IM7	Surface	Yes
^{172}Yb	CD4	RM4-5	Surface	No
^{173}Yb	CD117 (ckit)	2B8	Surface	Yes
^{174}Yb	MHC class II (IA/IE)	M5/114.15.2	Surface	No
^{175}Lu	CD127	A7R34	Surface	Yes
^{176}Yb	ICOS (CD278)	7E.17G9	Surface	Yes
^{195}Pt	Cisplatin	Cell-ID Cisplatin		No
^{191}Ir, ^{193}Ir	Intercalator	Cell-ID Intercalator-Ir		No
^{140}Ce ^{151}Eu ^{153}Eu ^{165}Ho ^{175}Lu	Normalization Beads			No

*Clustering parameters used for Figure 1 and 5 differed as indicated.

Table 2. Antibody conjugates used for the analysis in Figure 2.

Tag	Target	Ab Clone	Surface/Intracellular	Clustering*
^{89}Y	CD45	30-F11	Surface	Yes
^{141}Pr	Gr1 (Ly6C/Ly6G)	RB6-8C5	Surface	Yes
^{142}Nd	CD11c	N418	Surface	Yes
^{143}Nd	CD103-Biotin / anti-Biotin	2E7 (Biolegend) / 1D4C3 (anti-Biotin)	Surface	Yes
^{144}Nd	MHC class I	28-14-8	Surface	Yes
^{145}Nd	CD69	H1.2F3	Surface	Yes
^{146}Nd	CD8α	53-6.7	Surface	Yes
^{150}Nd	CD27	LG.3A10	Surface	Yes
^{151}Eu	CD25	3C7	Surface	Yes
^{152}Sm	CD3ε	145-2C11	Surface	Yes (A) / No (B-D)
^{154}Sm	CD11b	M1/70	Surface	Yes
^{156}Gd	CD49b-PE / anti-PE	HMa2 (Biolegend) / PE001 (anti-PE)	Surface/Secondary	Yes
^{159}Tb	PD-1 (CD279)	RMP1-30	Surface	Yes
^{160}Gd	KLRG1-FITC / anti-FITC	2FI (Thermo Fisher) / FIT-22 (anti-FITC)	Surface/Secondary	Yes
^{161}Dy	Tbet	4B10	Intracellular	Yes
^{162}Dy	Ly6C	HK1.4	Surface	Yes
^{163}Dy	Lag3-APC / anti-APC	C9B7W (Biolegend) / APC003 (anti-APC)	Surface/Secondary	Yes
^{164}Dy	IkBα	L35A5	Intracellular	Yes
^{166}Er	CD19	6D5	Surface	Yes
^{167}Er	CD150	TC15-12F12.2	Surface	Yes
^{168}Er	Ki-67	B56	Intracellular	Yes
^{169}Tm	IL10gfp	5F12.4 (anti-GFP)	Intracellular	Yes
^{170}Er	CD40L	MR1	Surface	Yes
^{171}Yb	CD44	IM7	Surface	Yes
^{172}Yb	CD4	RM4-5	Surface	Yes (A) / No (B-D)
^{173}Yb	CD117 (ckit)	2B8	Surface	Yes
^{174}Yb	MHC class II (IA/IE)	M5/114.15.2	Surface	Yes (A) / No (B-D)
^{175}Lu	CD127	A7R34	Surface	Yes
^{176}Yb	ICOS (CD278)	7E.17G9	Surface	Yes
^{195}Pt	Cisplatin	Cell-ID Cisplatin		No
^{191}Ir, ^{193}Ir	Intercalator	Cell-ID Intercalator-Ir		No
^{140}Ce ^{151}Eu ^{153}Eu ^{165}Ho ^{175}Lu	Normalization Beads			No

*Clustering parameters used for Figure 2B-D excluded CD3ε, CD4, and MHC class II.

Table 3. Antibody conjugates used for the analysis in Figure 3.

Tag	Target	Ab Clone	Surface/Intracellular	Clustering
^{89}Y	CD45	30-F11	Surface	Yes
^{141}Pr	pSHP2 [Y580]	D66F10	Intracellular	Yes
^{142}Nd	CD11c	N418	Surface	Yes
^{143}Nd	GITR (CD357)	DTA1	Surface	Yes
^{144}Nd	CXCR3-FITC / anti-FITC	CXCR3-173 (Biolegend)/ FIT-22 (anti-FITC)	Surface/Secondary	Yes
^{145}Nd	CD69	H1.2F3	Surface	Yes
^{146}Nd	CD8α	53-6.7	Surface	Yes
^{147}Sm	pHistone H2A.X (SER139)	JBW301	Intracellular	Yes
^{148}Nd	CD11b	M1/70	Surface	Yes
^{149}Sm	CD19	6D5	Surface	Yes
^{150}Nd	CD27	LG.3A10	Surface	Yes
^{151}Eu	CD25	3C7	Surface	Yes
^{152}Sm	CD3ε	145-2C11	Surface	No
^{153}Eu	PD-L1 (CD274)	10F.9G2	Surface	Yes
^{154}Sm	CTLA4 (CD152)	UC10-4B9	Intracellular	Yes
^{155}Gd	IRF4	3E4	Intracellular	Yes
^{156}Gd	41BB-PE / anti-PE	17B5 (Thermo Fisher) / PE001 (anti-PE)	Surface/Secondary	Yes
^{158}Gd	FoxP3	FJK-16s	Intracellular	Yes
^{159}Tb	PD-1 (CD279)	RMP1-30	Surface	Yes
^{160}Gd	CD5	53-7.3	Surface	Yes
^{161}Dy	Tbet	4B10	Intracellular	Yes
^{162}Dy	Tim3 (CD366)	RMT3-23	Surface	Yes
^{163}Dy	BCL6	K112-91	Intracellular	Yes
^{164}Dy	IkBα	L35A5	Intracellular	Yes
^{165}Ho	Beta-catenin (active)	D13A1	Intracellular	Yes
^{166}Er	Arginase-1	Polyclonal	Intracellular	Yes
^{167}Er	Gata3	TWAJ	Intracellular	Yes
^{168}Er	Ki-67	B56	Intracellular	Yes
^{169}Tm	IL10gfp	5F12.4 (anti-GFP)	Intracellular	Yes
^{170}Er	CD49b	HMa2	Surface	Yes
^{171}Yb	CD44	IM7	Surface	Yes
^{172}Yb	CD4	RM4-5	Surface	No
^{173}Yb	CD117 (ckit)	2B8	Surface	Yes
^{174}Yb	Lag3 (CD223)	C9B7W	Surface	Yes
^{175}Lu	CD127	A7R34	Surface	Yes
^{176}Yb	ICOS (CD278)	7E.17G9	Surface	Yes
^{209}Bi	MHC class II (IA/IE)	M5/114.15.2	Surface	No
^{195}Pt	Cisplatin	Cell-ID Cisplatin		No
^{191}Ir, ^{193}Ir	Intercalator	Cell-ID Intercalator-Ir		No
^{140}Ce ^{151}Eu ^{153}Eu ^{165}Ho ^{175}Lu	Normalization Beads			No

Table 4A. Antibody conjugates used for the analysis in the lung (Figures 4A, 4C, and 4E).

Tag	Target	Ab Clone	Surface/Intracellular	Clustering
^{89}Y	CD45	30-F11	Surface	No
^{141}Pr	Gr-1 (Ly6C/Ly6G)	RB6-8C5	Surface	Yes
^{142}Nd	CD11c	N418	Surface	Yes
^{143}Nd	GITR (CD357)	DTA1	Surface	Yes
^{144}Nd	MHC class I	28-14-8	Surface	Yes
^{145}Nd	CD69	H1.2F3	Surface	Yes
^{146}Nd	CD8α	53-6.7	Surface	Yes
^{148}Nd	CD11b	M1/70	Surface	Yes
^{149}Sm	p4E-BP1 [T37/T46]	236B4	Intracellular	Yes
^{150}Nd	CD25	3C7	Surface	Yes
^{151}Eu	CD64	X54-5/7.1	Surface	Yes
^{152}Sm	CD3ε	145-2C11	Surface	Yes
^{153}Eu	PD-L1 (CD274)	10F.9G2	Surface	Yes
^{154}Sm	CTLA4 (CD152)	UC10-4B9	Intracellular	Yes
^{155}Gd	IRF4	3E4	Intracellular	Yes
^{156}Gd	Siglec-F-PE / anti-PE	E50-2440 (BD Pharmingen) / PE001 (anti-PE)	Surface/Secondary	Yes
^{158}Gd	FoxP3	FJK-16s	Intracellular	Yes
^{159}Tb	PD-1 (CD279)	RMP1-30	Surface	Yes
^{160}Gd	KLRG1-FITC / anti-FITC	2FI (Thermo Fisher) / FIT-22 (anti-FITC)	Surface/Secondary	Yes
^{161}Dy	Tbet	4B10	Intracellular	Yes
^{162}Dy	Tim3 (CD366)	RMT3-23	Surface	Yes
^{163}Dy	Lag3-APC / anti-APC	C9B7W (Biolegend) / APC003 (anti-APC)	Surface/Secondary	Yes
^{164}Dy	IkBα	L35A5	Intracellular	Yes
^{165}Ho	Beta-catenin (active)	D13A1	Intracellular	Yes
^{166}Er	CD19	6D5	Surface	Yes
^{167}Er	NKp46	29A1.4	Surface	Yes
^{168}Er	Ki-67	B56	Intracellular	Yes
^{169}Tm	Ly-6A/E (Sca-1)	D7	Surface	Yes
^{170}Er	PD-L2-Biotin / anti-Biotin	TY25 (Biolegend) / 1D4-C5 (anti-Biotin)	Surface/Secondary	Yes
^{171}Yb	CD44	IM7	Surface	Yes
^{172}Yb	CD4	RM4-5	Surface	Yes
^{173}Yb	CD117 (ckit)	2B8	Surface	Yes
^{174}Yb	MHC class II (IA/IE)	M5/114.15.2	Surface	Yes
^{175}Lu	CD127	A7R34	Surface	Yes
^{176}Yb	ICOS	7E.17G9	Surface	Yes
^{195}Pt	Cisplatin	Cell-ID Cisplatin		No
^{191}Ir, ^{193}Ir	Intercalator	Cell-ID Intercalator-Ir		No
^{140}Ce ^{151}Eu ^{153}Eu ^{165}Ho ^{175}Lu	Normalization Beads			No

Table 4B. Antibody conjugates used for the analysis in the colon (Figures 4B, 4D, and 4F).

Tag	Target	Ab Clone	Surface/Intracellular	Clustering
^{89}Y	CD45	30-F11	Surface	No
^{141}Pr	Ly6G	1A8	Surface	Yes
^{142}Nd	CD11c	N418	Surface	Yes
^{143}Nd	CD103-Biotin / anti-Biotin	2E7 (Biolegend) / 1D4C3 (anti-Biotin)	Surface/Secondary	Yes
^{144}Nd	MHC class I	28-14-8	Surface	Yes
^{145}Nd	SiglecF-PE / anti-PE	E50-2440 (BD Pharmingen) / PE001 (anti-PE)	Surface/Secondary	Yes
^{146}Nd	CD8α	53-6.7	Surface	Yes
^{148}Nd	CD11b	M1/70	Surface	Yes
^{149}Sm	CD19	6D5	Surface	Yes
^{150}Nd	CD25	3C7	Surface	Yes
^{151}Eu	CD64	X54-5/7.1	Surface	Yes
^{152}Sm	CD3ε	145-2C11	Surface	Yes
^{153}Eu	PD-L1 (CD274)	10F.9G2	Surface	Yes
^{154}Sm	CTLA4 (CD152)	UC10-4B9	Intracellular	Yes
^{155}Gd	IRF4	3E4	Intracellular	Yes
^{156}Gd	CD90.2	30-H12	Surface	Yes
^{158}Gd	FoxP3	FJK-16s	Intracellular	Yes
^{159}Tb	RORgt	B2D	Intracellular	Yes
^{160}Gd	CXCR3-FITC / anti-FITC	CXCR3-173 (Biolegend) / FIT-22 (anti-FITC)	Surface/Secondary	Yes
^{161}Dy	Tbet	4B10	Intracellular	Yes
^{162}Dy	Ly6C	HK1.4	Surface	Yes
^{163}Dy	F4/80-APC / anti-APC	MB8 (Thermo Fisher) / APC003 (anti-APC)	Surface/Secondary	Yes
^{164}Dy	IkBα	L35A5	Intracellular	Yes
^{165}Ho	Beta-catenin (active)	D13A1	Intracellular	Yes
^{166}Er	Arginase-1	Polyclonal	Intracellular	Yes
^{167}Er	NKp46	29A1.4	Surface	Yes
^{168}Er	Ki-67	B56	Intracellular	Yes
^{169}Tm	Ly-6A/E (Sca-1)	D7	Surface	Yes
^{170}Er	CD49b	HMa2	Surface	Yes
^{171}Yb	CD44	IM7	Surface	Yes
^{172}Yb	CD4	RM4-5	Surface	Yes
^{173}Yb	CD117 (ckit)	2B8	Surface	Yes
^{174}Yb	Lag3 (CD223)	C9B7W	Surface	Yes
^{175}Lu	CD127	A7R34	Surface	Yes
^{176}Yb	ICOS (CD278)	7E.17G9	Surface	Yes
^{209}Bi	MHC class II (IA/IE)	M5/114.15.2	Surface	Yes
^{195}Pt	Cisplatin	Cell-ID Cisplatin		No
^{191}Ir, ^{193}Ir	Intercalator	Cell-ID Intercalator-Ir		No
^{140}Ce ^{151}Eu ^{153}Eu ^{165}Ho ^{175}Lu	Normalization Beads			No